JCTC Journal of Chemical Theory and Computation

Article

pubs.acs.org/JCTC

Structures and Energy Landscapes of Hydrated Sulfate Clusters

Lewis C. Smeeton,[†] James D. Farrell,[‡] Mark T. Oakley,[†] David J. Wales,[‡] and Roy L. Johnston*[,†]

[†]School of Chemistry, University of Birmingham, Edgbaston, Birmingham B15 2TT, United Kingdom

[‡]Department of Chemistry, University of Cambridge, Lensfield Road, Cambridge CB2 1EW, United Kingdom

Supporting Information

ABSTRACT: The sulfate ion is the most kosmotropic member of the Hofmeister series, but the chemical origins of this effect are unclear. We present a global optimization and energy landscape mapping study of microhydrated sulfate ions, $SO_4^{2-}(H_2O)_n$, in the size range $3 \leq n \leq 50$. The clusters are modeled using a rigid-body empirical potential and optimized using basin-hopping Monte Carlo in conjunction with a move set including cycle inversions to explore hydrogen bond topologies. For clusters containing a few water molecules ($n \leq 6$) we are able to reproduce *ab initio* global minima, either as global minima of the empirical potential, or as low-energy isomers. This result justifies applications to larger systems. Experimental studies have shown that dangling hydroxyl groups are present on the surfaces of pure water clusters, but absent in hydrated sulfate clusters up to $n \approx 43$. Our global optimization results agree with this observation, with dangling hydroxyl groups absent from the low-lying minima of small clusters, but competitive in larger clusters.

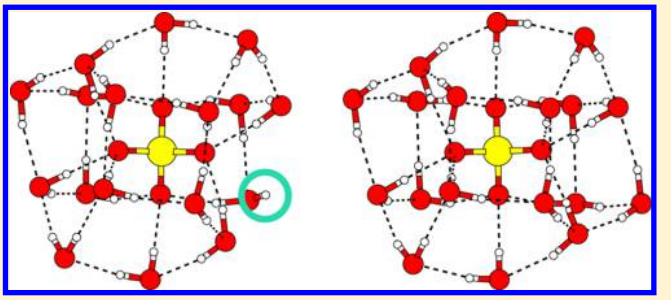

1. INTRODUCTION

The Hofmeister series ranks anions and cations according to their relative effectiveness at influencing a number of interesting phenomena in physical chemistry.[1,2] Within the series, ions can be characterized as being either kosmotropic (structure making) or chaotropic (structure breaking). Kosmotropes increase the surface tension of liquids[3] and the stability of proteins,[4] and decrease the solubility of hydrophobic particles[5] and the denaturation of proteins[6] (to name but a few properties), while chaotropes behave in the opposite manner.[7] However, despite the ubiquity of Hofmeister effects, their underlying chemical origins remain unclear, with theory and experiment seemingly providing evidence both for and against[3,8−10] the long-range structuring of solvent molecules around Hofmeister ions. The sulfate dianion sits at the far kosmotropic end of the Hofmeister series, and its solvation has been studied extensively by experiment[11−13] and theory,[14−18] due to its relevance in understanding the ordering behavior, as well as atmospheric chemistry,[19] and a number of industrial processes.

Infrared photodissociation (IRPD) spectroscopy of gas-phase hydrated sulfate clusters, $SO_4^{2-}(H_2O)_n$, in the size range $37 \leq n \leq 80$ has revealed a size dependence of the appearance of OH bonds protruding from the surface of the clusters. The experimental signature, a small peak in the IRPD spectra around 3700 cm^{-1}, is only observed for clusters with $n > 43$, indicating that, for smaller clusters, all OH bonds participate in an OH···O hydrogen bond.[11] This result contrasts with the surface of bulk water[20] and small water clusters,[21] where many water molecules are able to orient themselves to expose a dangling OH bond, and suggests that the sulfate ion has a significant effect on the surrounding water structure, even beyond the second solvation shell. Here we present a systematic computational study of $SO_4^{2-}(H_2O)_n$, in the range $3 \leq n \leq 50$, providing microscopic insight into the hydrogen bonding network of water molecules around the sulfate dianion and into the size-dependent emergence of dangling OH bonds.

2. METHODOLOGY

2.1. Modeling the System. Due to the relatively large system sizes under consideration, we have modeled the hydrated sulfate clusters using an empirical potential with bond lengths and bond angles held rigid. The water molecules are represented by the four-site rigid-body TIP4P water potential,[22] which includes the two hydrogen atoms, the oxygen atom, and a lone pair site. The O−H bond distance and H−O−H bond angle are 0.9572 Å and 104.52°, respectively, and the lone pair site lies 0.15 Å along the H−O−H bond angle bisector. Potential parameters are shown in Table 1.

TIP4P water clusters have been studied extensively,[21,23−31] with good candidate global minima determined for up to 36

Table 1. TIP4P Potential Parameters for H_2O[22]

atom	q_i/e	σ/Å	ε/kcal mol^{-1}
hydrogen	+0.52	0.0	0.0
oxygen	0.0	3.15	0.648
lone pair	−1.04	0.0	0.0

Received: December 4, 2014

DOI: 10.1021/acs.jctc.5b00151
J. Chem. Theory Comput. XXXX, XXX, XXX−XXX

water molecules,[27] and reasonable agreement with both *ab initio* calculations and experiment up to 12 molecules.[29] TIP4P water is also able to qualitatively describe the water phase diagram,[32,33] though modifications to the model exist which can give better quantitative agreement.[34] The sulfate dianion is modeled as a tetrahedral molecule with rigid S−O bonds of length 1.49 Å and O−S−O bond angles of 109.5°. The binding energy, U, of a cluster containing N atoms was computed as a sum of pairwise Coulombic and Lennard-Jones terms

$$U = \sum_{i=1}^{N} \sum_{j=i+1}^{N} \left\{ \frac{q_i q_j}{r_{ij}} + 4\varepsilon \left[\left(\frac{\sigma}{r_{ij}} \right)^{12} - \left(\frac{\sigma}{r_{ij}} \right)^{6} \right] \right\} \quad (1)$$

where i and j are the atom indices, q_i is the partial charge on atom i, r_{ij} is the distance between nonbonded atoms i and j, and σ and ε are Lennard-Jones parameters. Lennard-Jones parameters for interactions between unlike atom types were calculated using the Lorentz−Berthelot mixing rules. All energies in the paper are given in units of kcal mol^{-1}.

The sulfate potential that we have used was derived from Møller−Plesset MP4SDTQ level calculations by McCammon et al. and has been shown to reproduce experimental solution data.[14] Previous calculations of the microsolvation of the sulfate ion at the MP2 level also agree with the MP4 results.[17] McCammon et al. suggested two sulfate potentials, with the same Lennard-Jones parameters but different partial charges on the sulfur and oxygen atoms. In order to choose between these parameter sets, we performed short basin-hopping runs for $SO_4^{2-}(H_2O)_n$ in the size range $3 \le n \le 7$ for both potentials. The 40 lowest-energy isomers for each n were then reoptimized using density functional theory (DFT) level with the B3LYP exchange-correlation functional and a 6-311++G** basis set, as implemented within the NWChem package.[35] Little difference in isomer ordering was found when comparing the two potentials, so we chose to use the first of the two parameter sets suggested by McCammon et al. (Table 2) because it had a slightly better Spearman rank correlation with the DFT calculations.

Table 2. Potential Parameters for SO_4^{2-}[14]

atom	q_i/e	σ/Å	ε/kcal mol^{-1}
sulfur	+2.4	3.55	0.25
oxygen	−1.1	3.15	0.25

As both the water molecules and the sulfate anion are treated as rigid bodies, we have used angle-axis variables to describe the rigid-body rotational coordinates. This representation is preferred to Euler angles, since it avoids the problems in geometry optimization that arise from singularities when these coordinates are used.[36−38]

2.2. Global Optimization. Low-energy minima on the potential energy surface of $SO_4^{2-}(H_2O)_n$ were located using the basin-hopping algorithm[39−41] implemented in the GMIN[42] and pele[43] software packages. For each cluster in the range $3 \le n \le 50$, eight searches were conducted starting from different random geometries. The basin-hopping algorithm works as follows: (1) With an initial potential energy minimum as a starting point, the geometry is perturbed. (2) A local minimization of the geometry is performed with respect to the potential energy. (3) The new minimum is accepted or rejected according to a Metropolis criterion.[44]

The geometry was perturbed according to three distinct move classes: rigid-body translations of the center-of-mass of the water molecules and sulfate ion, rigid-body rotations about the oxygen atom (for the water molecules) or sulfur atom (for the sulfate ion), and cycle inversion moves (equivalent to Takeuchi's closed chain perturbations[24]). A cycle in a directed network is a closed loop of edges with the direction of each edge pointing the same way around the loop.[45] Such a loop can be inverted by pointing edges in the opposite direction. The cycle inversion move class searches for simple cycles (those in which no node appears twice) in the directed network of water−water hydrogen bonds using the `simple_cycles` method in `networkx`,[46] a Python library for the creation, manipulation, and study of networks. In a cycle inversion move, a cycle is chosen at random from the hydrogen bond network and inverted. If no cycles are present, a rigid-body translation or rotation is performed instead. A water molecule i is considered to donate a hydrogen bond to water molecule j if their oxygen−oxygen distance is less than 3.50 Å and the OH bond axis of molecule i is within 30° of the displacement vector between the oxygen atoms in i and j. Some structures with positively charged atoms close to the TIP4P lone pair underwent cold fusion. These structures were discarded from the basin-hopping search.

Global optimization studies of pure water clusters have suggested that the use of block moves, where one type of move class is used exclusively for a set number of steps before switching to another, is an effective strategy for finding low-energy structures.[30] In this study, we used blocks of 100 steps for each type of move. To ensure reasonable parameters for searching across a variety of n, we tuned the size of the translation step and the temperature used in the Metropolis acceptance criterion. This tuning was achieved by running 160 000 basin-hopping steps for each parameter combination for every tenth cluster size starting from $n = 5$ (i.e., $n = 5$, 15, 25, ...). The combination of temperature and translational step size that consistently found the lowest-energy minima was considered to be optimal, and was assumed to be transferable to neighboring sizes.

2.3. Energy Landscape Mapping. Transition states connecting minima on the potential energy surface of small hydrated sulfate clusters were located using the pele software package.[43] A doubly nudged elastic band method[47] was used to find transition state candidates, with interpolation between end points using a linear interpolation of the translational coordinates of the rigid-body molecules and spherical linear quaternion interpolation of the rotational coordinates.[48] Transition state candidates were further optimized with hybrid eigenvector-following.[49,50] Initially, connection attempts were made between pairs of minima chosen at random, or between a randomly chosen minimum and the global minimum. Later, we adopted a strategy to remove artificial frustration in the network by attempting to connect minima to the global minimum, according to a weighting proportional to the barrier separating the two minima divided by their difference in energy.[51] The energy landscapes were visualized as disconnectivity graphs[52,53] using the PyConnect software package.[54] Analysis of clusters with $n = 9$ and $n = 12$ is presented here, and disconnectivity graphs for other clusters in the range $3 \le n \le 12$ are available in the Supporting Information.

DOI: 10.1021/acs.jctc.5b00151
J. Chem. Theory Comput. XXXX, XXX, XXX−XXX

3. RESULTS AND DISCUSSION

For clusters with $n \leq 18$, all eight basin-hopping runs located the same lowest common energy minimum, and for $n = 19$, seven of the eight basin-hopping runs located the same lowest common energy minimum. For $n = 19$, approximately 1.2 million energy minimizations were conducted, requiring $\approx 3.4 \times 10^9$ energy evaluations. These structures are probably good candidates for global minima (Figure 1). For $n \geq 20$, none of the eight basin-hopping runs locate a common lowest-energy structure, and so the putative "global minima" presented at this size have been observed by only one of the independent basin-hopping searches. Hence, they may be representative of low-lying minima, rather than the true global minimum. This is a sharp decrease in search success. To investigate further, at each cluster size in the range $16 \leq n \leq 21$ (i.e., 3 water molecules either side of the transition) we performed 100 basin-hopping searches of 300 000 steps each and found that the effect persists over the larger number of searches. Studying the geometry of low-energy minima on either side of the drop-off does not reveal any obvious feature that might inhibit search success, and so the sharp fall could be a result of the increasing dimensionality of the search space (for a rigid-body molecular system such as this, the number of degrees of freedom increases by 6, not 3, for each water molecule added). The statistics for the successful searches are reported in the Supporting Information. It should be noted that the calculations reported here do not include zero-point vibrational energies, and it has been shown that some reordering of the isomer energies can occur when they are considered.[15,55]

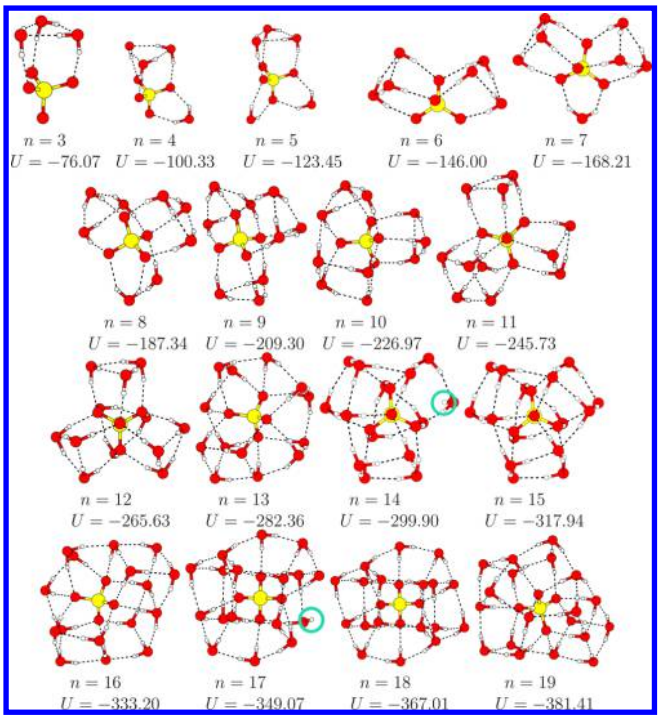

Figure 1. Structures and binding energy, U, values of the putative global minima for $SO_4^{2-}(H_2O)_n$ clusters where $3 \leq n \leq 19$. The semidangling OH bonds in $n = 14$ and 17 are highlighted. Structures of the putative global minima for $3 \leq n \leq 50$ are given in the Supporting Information. Energies are in kcal mol^{-1}.

Global minima of $SO_4^{2-}(H_2O)_n$ for $n \leq 7$ have been presented in a previous study by Head-Gordon et al.[15] using a combined empirical potential/DFT search method. Our global minima for $n = 4$ and 5 agree with the DFT results (minima 4.5.3 and 5.7.3 in ref 15, respectively), and the DFT global minima for $n = 3$ and 6 (minima 3.6.0 and 6.7.5 in ref 15, respectively) are low-energy isomers (but not global minima) for the present potential. We were unable to reproduce the structure previously proposed as the global minimum for $n = 7$ (minimum 7.9.5 in ref 15). However, when treated at the DFT level using the B3LYP exchange-correlation functional and 6-311++G** basis set, this structure rearranged to a different geometry, previously reported as the third minimum, which we did find in our global optimization study. Our empirical global minimum for $n = 7$ is also the lowest energy structure when relaxed and evaluated at the DFT level, and corresponds to the second lowest DFT isomer previously reported (minimum 7.8.6 in ref 15). To the best of our knowledge, global minima for $n \geq 8$ have not been reported in the literature, so for clusters above this size we have no previous results for a comparison. The evolution of the energy per water molecule, $U(n)/n$ (Figure 2), suggests that $n = 50$ is not sufficient to have reached the asymptotic limit of the bulk, infinitely dilute, solution.

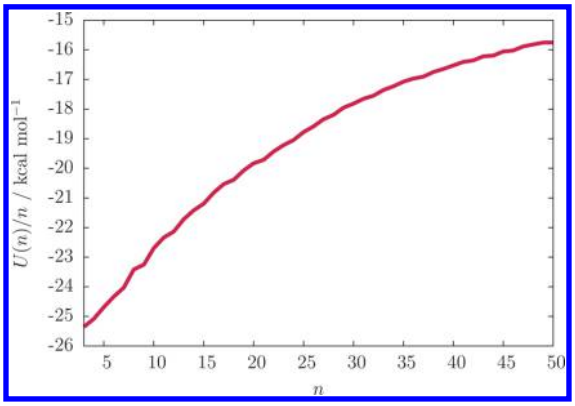

Figure 2. Energy per water of the putative global minima of $SO_4^{2-}(H_2O)_n$ clusters, $U(n)/n$, as a function of the number of water molecules, n, for $3 \leq n \leq 50$.

We can identify particularly stable cluster sizes using the central difference approximation to the second derivative of $U(n)$, Figure 3:

$$\Delta_2 U(n) = \frac{1}{2}[U(n+1) + U(n-1)] - U(n) \quad (2)$$

The more positive $\Delta_2 U(n)$ is, the more stable that structure is relative to its next nearest neighboring sizes. In the size range $3 \leq n \leq 15$, the more stable structures are those that contain a high proportion of trimeric water rings ($n = 7$, 9, 12, 15). For $24 \leq n \leq 50$ we observe alternating even−odd behavior, with structures containing even numbers of water molecules being more stable. This result contrasts with the behavior of homogeneous TIP4P water,[21] where even−odd behavior is observed for smaller clusters, before it disappears at larger sizes.

In Figure 4 we plot the mean hydrogen bond length between pairs of water molecules, r_{OH}^{ww}, and between a water molecule and one oxygen of the sulfate ion, r_{OH}^{ws}, of the global minima as a function of n. r_{OH}^{ww} is consistent with the mean hydrogen bond length in pure TIP4P water clusters, and r_{OH}^{ws} is ≈4% shorter than r_{OH}^{ww} for all n. An exception to this trend occurs at $n = 5$, where the mean is skewed by the long hydrogen bonds between

DOI: 10.1021/acs.jctc.5b00151
J. Chem. Theory Comput. XXXX, XXX, XXX−XXX

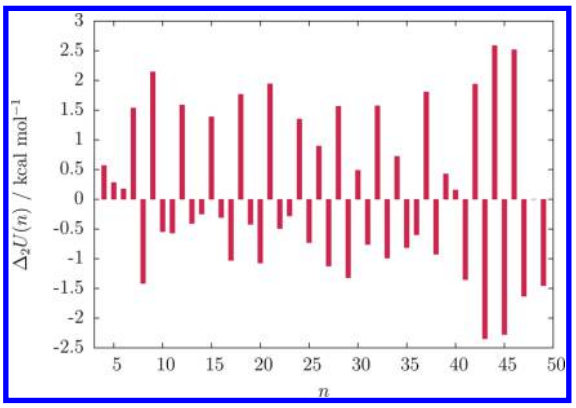

Figure 3. Central difference approximation to the second derivative of the energy of the putative global minima, $\Delta_2 U(n)$, as a function of n.

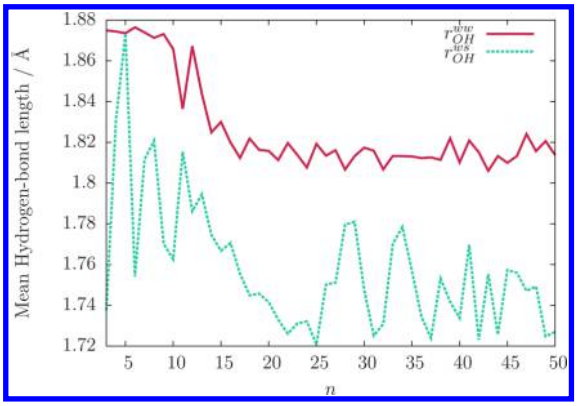

Figure 4. Mean hydrogen bond length between water molecules, r_{OH}^{ww}, and between water and the sulfate ion, r_{OH}^{ws}, for the putative global minimum structures of $SO_4^{2-}(H_2O)_n$ clusters as a function of the number of water molecules, n, shown in red and green, respectively.

the two water molecules bonded along the edge of the sulfate. The comparative shortening of hydrogen bonds between water molecules and the sulfate is presumably due to the larger partial charge on the oxygen atom in the sulfate ion than on the lone pair in the TIP4P water. The shortening of r_{OH}^{ws} in the range $13 \leq n \leq 25$ is probably due to the compression of the inner water shell in order to allow for tangential hydrogen bonding between water molecules that might otherwise be too far apart. Fluctuations between 12 and 14 coordination of the sulfate ion are responsible for the oscillatory behavior in r_{OH}^{ws} above $n = 25$. Here, we define the length of a hydrogen bond to be the OH···O distance.

In order to study the size-dependent appearance of dangling OH bonds, we examined the hydrogen bonding network of water molecules and the sulfate ion. We deemed structures with a water molecule donating only a single hydrogen bond, either to another water molecule or to the sulfate ion, to contain a dangling OH bond. Dangling OH bonds protruding radially from the cluster were observed in the global minimum structures for the larger hydrated sulfate clusters at $n = 43$, 45, and 47. In the smaller clusters $n = 14$ and 17, we observe semidangling OH bonds, which do not engage in a hydrogen bond, but do not protrude radially from the cluster surface. Subsequent local minimizations of these structures at the DFT level (B3LYP, 6-311++G**) show that these semidangling OH groups remain and are not an artifact of the potential. We define $\bar{f}$ as the Boltzmann-weighted mean number of dangling OH bonds

$$\bar{f} = \sum_i \frac{e^{-\Delta U_i \beta} f_i}{e^{-\Delta U_i \beta}} \tag{3}$$

where f_i and ΔU_i are the number of dangling OH bonds and energy above the global minimum for minimum i, respectively, and $\beta \equiv 1/k_B T$. The sum is taken over all unique structures found during any one of the independent basin-hopping global optimization searches or (for $3 \leq n \leq 12$) in transition state searches. In Figure 5 we plot $\bar{f}$ as a function of n, weighted by

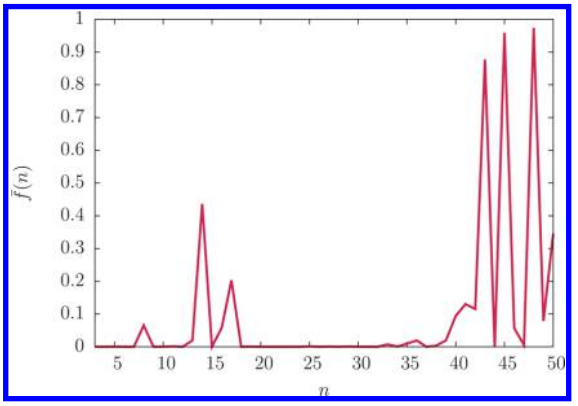

Figure 5. Boltzmann-weighted mean number of dangling OH bonds, $\bar{f}$, as a function of the number of water molecules, n, for $3 \leq n \leq 50$.

temperature, $T = 130$ K, to be consistent with experiment,[11] and assume that at this temperature the free energy can be estimated from the potential energy alone (i.e., that the entropic contribution to the free energy from each isomer is approximately the same). For the size range $3 \leq n \leq 19$ there are three peaks in $\bar{f}$ at $n = 8$, 14, and 17 water molecules, due to the global minima of $n = 14$ and 17 exhibiting a dangling OH bond each. For $SO_4^{2-}(H_2O)_8$, there exist a number of low-energy isomers with one or two dangling OH bonds, which are stabilized by the other water molecules participating in two trimeric water rings. For $20 \leq n \leq 39$ we observe no energetically relevant structures exhibiting a dangling OH bond. For $40 \leq n \leq 50$ we begin to observe system sizes with prevalent numbers of dangling OH bonds more frequently, with $\bar{f} \approx 0.9$ at $n = 43$, 45, and 48. At this stage, it is not obvious whether the pseudo-odd−even behavior of $\bar{f}$ in this size range is physical, or an artifact due to the difficulty of sampling structures at this size. Provisionally, the data is consistent with the IRPD spectra of size-selected hydrated sulfate clusters,[11] which indicate that the sulfate ion suppresses the appearance of dangling OH bonds until $n \approx 43$.

This suppression is not currently well-understood, but we can begin to rationalize it as follows: a water molecule is capable of donating and accepting up to two hydrogen bonds (i.e., four hydrogen bonds in total). In order for a water-containing system to totally inhibit the appearance of dangling OH bonds, each water *must* donate both OH bonds into a hydrogen bond. For systems solely composed of water molecules, this can only be achieved in highly coordinated environments such as bulk ice. At surfaces or in clusters, such coordination numbers are unachievable, and thus dangling OH bonds appear. In hydrated sulfate clusters, the sulfate anion occupies the center of the cluster, favoring highly coordinated

DOI: 10.1021/acs.jctc.5b00151
J. Chem. Theory Comput. XXXX, XXX, XXX−XXX

sites. When the first solvation shell is filled, it is able to accept 12−14 hydrogen bonds without donating any back into the system. In this manner, the sulfate anion acts as a net sink for hydrogen bonds, relaxing the requirement that the mean number of donated and accepted hydrogen bonds must be the same. We define $\overline{r}_{ad}$ to be the ratio of the Boltzmann-weighted mean number of hydrogen bonds accepted by and donated to a water molecule

$$\overline{r}_{ad} = \sum_i \frac{e^{-\Delta U_i \beta} a_i / d_i}{e^{-\Delta U_i \beta}} \quad (4)$$

where a_i and d_i are the number of hydrogen bonds accepted by and donated to a water molecule in minima i respectively, and ΔU_i is the energy of minimum i above the global minimum. In Figure 6 we plot $\overline{r}_{ad}$ as a function of the number of water

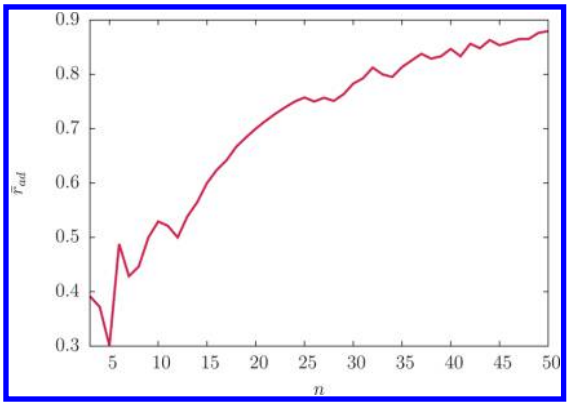

Figure 6. Ratio of the Boltzmann-weighted mean number of hydrogen bonds accepted by and donated to a water molecule, $\overline{r}_{ad}$, as a function of the number of water molecules, n, for $3 \leq n \leq 50$.

molecules n, and observe that for small n, $\overline{r}_{ad}$ is approximately 0.5 (i.e., a water molecule on average donates twice as many hydrogen bonds as it accepts). As the system size increases, the significance of the sulfate ion as a net hydrogen bond acceptor decreases, with $\overline{r}_{ad}$ rising to ≈0.9 at $n = 50$, implying that 90% of hydrogen bonds are being accepted by water molecules. Note that, for systems composed entirely of water molecules (or in the limit of an infinitely dilute solution), $\overline{r}_{ad} = 1$. Though this analysis provides some insight into the size-dependent inhibition of dangling OH bonds, it is still not clear why they should begin to appear around 40 water molecules and above, and this will be the focus of future work.

3.1. Structural Analysis of Global Minima and Energy Landscapes for $3 \leq n \leq 12$. Common structural motifs for the structures of the global minima of $SO_4^{2-}(H_2O)_n$ for $3 \leq n \leq 12$ are trimeric water rings about the open faces of the sulfate ion, with the water molecules in $n = 3, 6, 9, 12$ all engaged exclusively in such rings. There is some dispute regarding the size-dependent appearance of the second solvation shell, with estimates placed between 8 and 12 water molecules.[56,57] If we define the second solvation shell as beginning when a water molecule hydrogen bonds only with other water molecules (and not the sulfate ion), we find that the onset is ambiguous. In the lowest energy structures with $n = 10$ and 11, we observe a water molecule which hydrogen bonds only with other water molecules, and participates in a tetrameric ring instead of bonding onto the exposed face of the sulfate ion. At $n = 12$ all water molecules return to sharing a hydrogen bond with the sulfate ion, but for sizes larger than this, at least one water molecule is hydrogen bonded to other waters only.

We built databases of minima and transition states for clusters in the size range $3 \leq n \leq 12$, and present results for $n = 9$ and $n = 12$, which contain 12 094 minima and 144 677 transition states and 14 419 minima and 228 415 transition states, respectively, and display interesting kinetic features. Data for other sizes can be found in the Supporting Information. Figures 7 and 8 show the disconnectivity graph and two lowest-

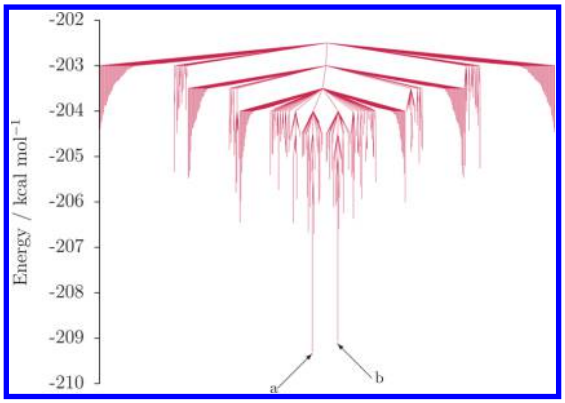

Figure 7. Disconnectivity graph for $SO_4^{2-}(H_2O)_9$ containing 555 minima and 1182 transition states connected to the global minimum below −202.5 kcal mol^{-1}.

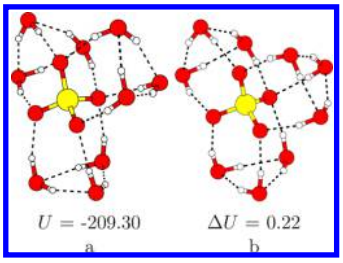

Figure 8. $SO_4^{2-}(H_2O)_9$ global minimum (a) and the next lowest-energy isomer (b), as labeled in the disconnectivity graph in Figure 7. ΔU is the energy of a given isomer above the global minimum. Energies are in kcal mol^{-1}.

energy isomers of $SO_4^{2-}(H_2O)_9$, respectively. The two isomers both have three trimeric hydrogen bonded water rings (i.e., the same oxygen skeleton), but differ in the relative directionality of the hydrogen bonded rings, resulting in an energy difference of $\Delta U = 0.22$ kcal mol^{-1}. In spite of the energetic and structural similarity, the two isomers are separated by a barrier of ≈6 kcal mol^{-1}, leading to a frustrated landscape. The relationship between low-energy isomers that share an oxygen skeleton but differ in hydrogen bond directionality is observed for clusters of other sizes. The disconnectivity graph for $SO_4^{2-}(H_2O)_{12}$ is shown in Figure 9, with the five lowest-energy isomers labeled and their structures shown in Figure 10. The isomers are organized into two oxygen skeletons, differing in the relative directionality of the hydrogen bonding in the rings alone. Isomers a, d, and e have four trimeric hydrogen bonded water rings, and isomers b and c have structures with one trimeric ring and a nine-membered water cycle. Both oxygen skeletons contain 12 water−sulfate and 12 water−water hydrogen bonds. As with the $n = 9$ system, large energetic barriers exist between the isomers, which will lead to frustrated kinetics. In both systems, the energetic gap (≈2.5 kcal mol^{-1} and ≈1.5 kcal

DOI: 10.1021/acs.jctc.5b00151
J. Chem. Theory Comput. XXXX, XXX, XXX−XXX

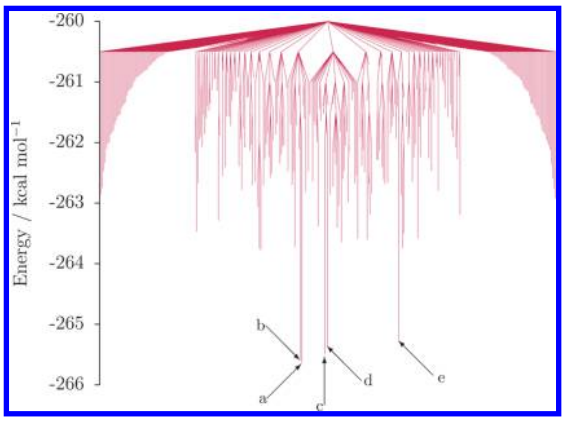

Figure 9. Disconnectivity graph for $SO_4^{2-}(H_2O)_{12}$ containing 335 minima and 390 transition states connected to the global minimum below −260.0 kcal mol^{-1}.

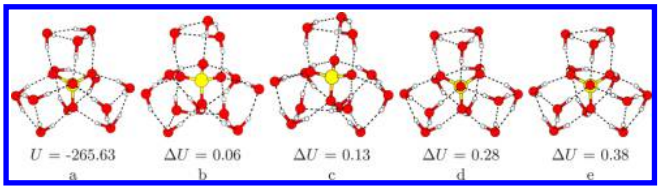

Figure 10. $SO_4^{2-}(H_2O)_{12}$ global minimum (a) and the next four lowest-energy isomers (b−e), as labeled on the disconnectivity graph in Figure 9. ΔU is the energy of a given isomer above the global minimum. Energies are in kcal mol^{-1}.

mol^{-1} for n = 9 and n = 12, respectively) between the labeled minima and the next lowest-energy isomer suggests that the oxygen skeleton geometry is the key factor in determining the energy of hydrated clusters in this size range.

3.2. Structural Analysis of Global Minima for 13 ≤ *n* ≤ 19. For clusters with $n \geq 13$, we begin to see 3-fold symmetric concave caps of six water molecules about the vertex of the sulfate (three water molecules hydrogen bond to an oxygen atom on the sulfate and the other three hydrogen bonds between them, see n = 18 for an illustration). One and two concave caps are observed for n = 15 and 18, respectively, and feature in the global minima and low-energy isomers for many of the larger cluster sizes. Search methods that bias toward such caps may prove to be a useful optimization strategy for future studies of hydrated sulfate clusters. Clusters containing n = 14 and n = 17 waters feature a single semidangling OH bond, and are the only two global minimum structures found in our study below n = 43 to do so. In both cases, the structures are similar to their n + 1 neighboring global minimum, but with a water molecule missing from the concave cap, causing one of the water molecules to have a dangling OH bond. It should be noted that the dangling OH bond belongs to a water molecule in the first solvation shell, and donates a hydrogen bond directly to the sulfate ion. Analysis of the normal-mode frequencies of these unusual structures confirms that they are minima on their respective potential energy surfaces.

The largest cluster size at which a trimeric water-ring appears around the open face of the sulfate ion is n = 15. For $n \geq 16$ (with the exception of n = 17 which has a dangling water), the graph of hydrogen bonded water molecules is connected, and there are no self-contained subnetworks of water molecules that hydrogen bond to either themselves or the sulfate (for example, the four trimeric water rings in n = 12 are each disconnected from the other). Water "cubes" are observed,[31,58,59] which share an edge with the sulfate ion (see n = 16 and n = 19). The largest cluster for which the same putative global minimum is found consistently by the majority of independent basin-hopping searches is n = 19.

3.3. Structural Analysis of Hydrated Sulfate Clusters for 20 ≤ *n* ≤ 50. For each cluster with $n \geq 20$, the putative global minimum is found in only a single search, so we are not confident that they are the global minima, but we believe that they are structurally representative of low-energy isomers. Structures of putative global minima for $3 \leq n \leq 50$ are given in the Supporting Information. Minima containing one, two, or three concave caps are a recurring feature, along with structures that appear for the homogeneous TIP4P water clusters, including fused cubes and edge-sharing pentagonal prisms.[30] The sulfate remains fairly central within the cluster throughout. The most important feature is that we do not see the emergence of dangling OH bonds in any of the global minima or low-energy isomers until $n \approx 40$, with f growing from 0 to ≈0.9 (Figure 5). The suppression of dangling OH bonds, and the cluster size at which they begin to appear, is roughly equivalent to what is found in the experimental IRPD spectra.

3.4. Conclusions. Microhydrated ions are interesting systems both experimentally and computationally for investigating the influence of ions on local water structure. We have shown that rigid-body modeling of hydrated sulfate clusters is capable of replicating the physical chemistry of these systems. For clusters containing a few water molecules ($n \leq 6$), we are able to reproduce *ab initio* global minima, either as global minima of the empirical potential, or as low-energy isomers. In the size range $3 \leq n \leq 12$, the structures of low-energy minima exhibit water molecules engaging in trimer water rings. The global minima for n = 3, 6, 9, and 12 water molecules are particularly stable, with the water molecules participating in such rings exclusively. For these systems, the lowest energy isomers typically have the same oxygen skeleton, but with different relative directionality of the hydrogen bonds, as explored with cycle inversion moves. Landscape analysis reveals that although these structures differ only slightly in energy, the barriers to interconversion can be very large, suggesting that such systems will display frustrated kinetics. At larger cluster sizes we note that dangling OH bonds are unfavorable up to n ≈ 43, consistent with IRPD spectra of size-selected clusters. We suggest that this is due to the sulfate ion acting as a net acceptor of hydrogen bonds, which allows water molecules in the system to accept only a fraction of the hydrogen bonds that they donate.

Future work will involve global optimization of hydrated sulfate clusters directly at the *ab initio* level using the BCGA-DFT code[60,61] and a combined DFT/basin-hopping[62] approach. We will also extend this work to study other microhydrated Hofmeister ions.

■ ASSOCIATED CONTENT

Supporting Information

Structures of the putative global minima for $SO_4^{2-}(H_2O)_n$ in the size range $3 \leq n \leq 50$, disconnectivity trees for $SO_4^{2-}(H_2O)_n$ in the size range $3 \leq n \leq 8$ and $10 \leq n \leq 11$, and search success statistics. This material is available free of charge via the Internet at http://pubs.acs.org.

DOI: 10.1021/acs.jctc.5b00151
J. Chem. Theory Comput. XXXX, XXX, XXX−XXX

AUTHOR INFORMATION

Corresponding Author

*E-mail: r.l.johnston@bham.ac.uk.

Notes

The authors declare no competing financial interest.

ACKNOWLEDGMENTS

We acknowledge the Engineering and Physical Sciences Research Council, UK (EPSRC), for funding under Programme Grant EP/I001352/1. Computational facilities were provided by the MidPlus Regional Centre of Excellence for Computational Science, Engineering and Mathematics, under EPSRC Grant EP/K000128/1 and the University of Birmingham's BlueBEAR HPC service, which provides a High-Performance Computing service to the University's research community. See http://www.birmingham.ac.uk/bear for more details. The authors thank Dr. Jacob Stevenson (University of Cambridge) for advice and guidance with the pele code and Dr. Sven Heiles and Prof. Evan Williams (U.C. Berkeley) for their experimental input and helpful comments.

REFERENCES

(1) Kunz, W.; Lo Nostro, P.; Ninham, B. *Curr. Opin. Colloid Interface Sci.* **2004**, *9*, 1−18.
(2) Hofmeister, F. *Arch. Exp. Pathol. Pharmakol.* **1888**, *24*, 247−260.
(3) Pegram, L. M.; Record, M. T. *J. Phys. Chem. B* **2007**, *111*, 5411−5417.
(4) Baldwin, R. L. *Biophys. J.* **1996**, *71*, 2056−2063.
(5) Russo, D. *Chem. Phys.* **2008**, *345*, 200−211.
(6) Levy-Sakin, M., Scherzer-Attali, R., Gazit, E. *Protein and Peptide Folding, Misfolding, and Non-Folding*; John Wiley & Sons, Inc.: New York, 2012; pp 441−478.
(7) Zhang, Y.; Cremer, P. S. *Curr. Opin. Chem. Biol.* **2006**, *10*, 658−663.
(8) Smith, J. D.; Saykally, R. J.; Geissler, P. L. *J. Am. Chem. Soc.* **2007**, *129*, 13847−13856.
(9) Freire, M. G.; Neves, C. M. S. S.; Silva, A. M. S.; Santos, L. M. N. B. F.; Marrucho, I. M.; Rebelo, L. P. N.; Shah, J. K.; Maginn, E. J.; Coutinho, J. A. P. *J. Phys. Chem. B* **2010**, *114*, 2004−2014.
(10) Uejio, J. S.; Schwartz, C. P.; Duffin, A. M.; Drisdell, W. S.; Cohen, R. C.; Saykally, R. J. *Proc. Natl. Acad. Sci. U.S.A.* **2008**, *105*, 6809−6812.
(11) O'Brien, J. T.; Prell, J. S.; Bush, M. F.; Williams, E. R. *J. Am. Chem. Soc.* **2010**, *132*, 8248−8249.
(12) Bush, M. F.; Saykally, R. J.; Williams, E. R. *J. Am. Chem. Soc.* **2007**, *129*, 2220−2221.
(13) Yang, X.; Wang, X.-B.; Wang, L.-S. *J. Phys. Chem. A* **2002**, *106*, 7607−7616.
(14) Cannon, W. R.; Pettitt, B. M.; McCammon, J. A. *J. Phys. Chem.* **1994**, 6225−6230.
(15) Lambrecht, D. S.; Clark, G. N. I.; Head-Gordon, T.; Head-Gordon, M. *J. Phys. Chem. A* **2011**, *115*, 11438−11454.
(16) Mardirossian, N.; Lambrecht, D. S.; McCaslin, L.; Xantheas, S. S.; Head-Gordon, M. *J. Chem. Theory Comput.* **2013**, *9*, 1368−1380.
(17) Pye, C. C.; Rudolph, W. W. *J. Phys. Chem. A* **2001**, *105*, 905−912.
(18) Jungwirth, P.; Curtis, J. E.; Tobias, D. *J. Chem. Phys. Lett.* **2003**, *367*, 704−710.
(19) Ramanathan, V.; Crutzen, P. J.; Kiehl, J. T.; Rosenfeld, D. *Science* **2001**, *294*, 2119−2124.
(20) Du, Q.; Superfine, R.; Freysz, E.; Shen, Y. *Phys. Rev. Lett.* **1993**, *70*, 2313−2316.
(21) Kazachenko, S.; Thakkar, A. J. *J. Chem. Phys.* **2013**, *138*, 194302.
(22) Jorgensen, W. L.; Chandrasekhar, J.; Madura, J. D.; Impey, R. W.; Klein, M. L. *J. Chem. Phys.* **1983**, *79*, 926.
(23) Kazachenko, S.; Thakkar, A. *J. Chem. Phys. Lett.* **2009**, *476*, 120−124.
(24) Takeuchi, H. *J. Chem. Inf. Model.* **2008**, *48*, 2226−2233.
(25) Kabrede, H. *Chem. Phys. Lett.* **2006**, *430*, 336−339.
(26) Hartke, B. *Z. Phys. Chem* **2000**, *214*, 1251.
(27) Kazachenko, S.; Thakkar, A. *J. Mol. Phys.* **2010**, *108*, 2187−2193.
(28) Kazimirski, J. K.; Buch, V. *J. Phys. Chem. A* **2003**, *107*, 9762−9775.
(29) Kabrede, H.; Hentschke, R. *J. Phys. Chem. B* **2003**, *107*, 3914−3920.
(30) Wales, D. J.; Hodges, M. P. *Chem. Phys. Lett.* **1998**, *286*, 65−72.
(31) Tsai, C. J.; Jordan, K. D. *J. Phys. Chem.* **1993**, *97*, 5208−5210.
(32) Sanz, E.; Vega, C.; Abascal, J. L. F.; MacDowell, L. G. *J. Chem. Phys.* **2004**, *121*, 1165−6.
(33) Sanz, E.; Vega, C.; Abascal, J.; MacDowell, L. *Phys. Rev. Lett.* **2004**, *92*, 255701.
(34) Abascal, J. L. F.; Vega, C. *J. Chem. Phys.* **2005**, *123*, 234505.
(35) Valiev, M.; Bylaska, E. J.; Govind, N.; Kowalski, K.; Straatsma, T. P.; van Dam, H. J. J.; Wang, D.; Nieplocha, J.; Apra, E.; Windus, T. L.; de Jong, W. A. *Comput. Phys. Commun.* **2010**, *181*, 1477−1489.
(36) Wales, D. J. *Philos. Trans. R. Soc., A* **2005**, *363*, 357−377.
(37) Chakrabarti, D.; Wales, D. J. *Phys. Chem. Chem. Phys.* **2009**, *11*, 1970−1976.
(38) Ruehle, V.; Kusumaatmaja, H.; Chakrabarti, D.; Wales, D. J. *J. Chem. Theory Comput.* **2013**, *9*, 4026−4034.
(39) Li, Z.; Scheraga, H. A. *Proc. Natl. Acad. Sci. U.S.A.* **1987**, *84*, 6611−6615.
(40) Wales, D. J.; Doye, J. P. K. *J. Phys. Chem. A* **1997**, *101*, 5111−5116.
(41) Wales, D. J.; Scheraga, H. A. *Science* **1999**, *285*, 1368−1372.
(42) GMIN: A program for finding global minima and calculating thermodynamic properties from basin-sampling. Available at http://www-wales.ch.cam.ac.uk/software.html.
(43) Python Energy Landscape Explorer. Available at http://github.com/pele-python/pele.
(44) Metropolis, N.; Rosenbluth, A. W.; Rosenbluth, M. N.; Teller, A. H.; Teller, E. *J. Chem. Phys.* **1953**, *21*, 1087−1092.
(45) Newman, M. *Networks: An Introduction*; Oxford University Press, Inc.: New York, 2010; pp 118−121.
(46) Hagberg, A. A.; Schult, D. A.; Swart, P. J. Exploring network structure, dynamics, and function using NetworkX. *Proceedings of the 7th Python in Science Conference (SciPy2008)*; Pasadena, CA, 2008; pp 11−15.
(47) Trygubenko, S. A.; Wales, D. J. *J. Chem. Phys.* **2004**, *120*, 2082−2094.
(48) Shoemake, K. Animating rotation with quaternion curves. *SIGGRAPH Comput. Graph.* **1985**, *19*, 245−254.
(49) Henkelman, G.; Jónsson, H.; Jonsson, H. *J. Chem. Phys.* **1999**, *111*, 7010−7022.
(50) Munro, L. J.; Wales, D. J. *Phys. Rev. B* **1999**, *59*, 3969−3980.
(51) Strodel, B.; Whittleston, C. S.; Wales, D. J. *J. Am. Chem. Soc.* **2007**, *129*, 16005−16014.
(52) Becker, O. M.; Karplus, M. *J. Chem. Phys.* **1997**, *106*, 1495.
(53) Wales, D. J.; Miller, M. A.; Walsh, T. R. *Nature* **1998**, *394*, 758−760.
(54) Smeeton, L. C.; Oakley, M. T.; Johnston, R. L. *J. Comput. Chem.* **2014**, *35*, 1481−1490.
(55) Miller, Y.; Chaban, G. M.; Zhou, J.; Asmis, K. R.; Neumark, D. M.; Gerber, R. B. *J. Chem. Phys.* **2007**, *127*, 094305.
(56) Gao, B.; Liu, Z.-f. *J. Chem. Phys.* **2005**, *123*, 224302.
(57) Wan, Q.; Spanu, L.; Galli, G. *J. Phys. Chem. B* **2012**, *116*, 9460−9466.
(58) Wales, D. J.; Ohmine, I. *J. Chem. Phys.* **1993**, *98*, 7257−7268.
(59) Wales, D. J.; Ohmine, I. *J. Chem. Phys.* **1993**, *98*, 7245−7256.
(60) Heiles, S.; Logsdail, A. J.; Schäfer, R.; Johnston, R. L. *Nanoscale* **2012**, *4*, 1109−1115.
(61) Heiles, S.; Johnston, R. L. *Int. J. Quantum Chem.* **2013**, *113*, 2091−2109.

DOI: 10.1021/acs.jctc.5b00151
J. Chem. Theory Comput. XXXX, XXX, XXX−XXX

(62) Do, H.; Besley, N. A. *J. Chem. Phys.* **2012**, *137*, 134106.

DOI: 10.1021/acs.jctc.5b00151
J. Chem. Theory Comput. XXXX, XXX, XXX−XXX